Sensors and Actuators A 197 (2013) 76–87

Contents lists available at SciVerse ScienceDirect

Sensors and Actuators A: Physical

journal homepage: www.elsevier.com/locate/sna

Motion control of piezoceramic actuators with creep, hysteresis and vibration compensation

Guo-Ying Gu, Li-Min Zhu*

State Key Laboratory of Mechanical System and Vibration, School of Mechanical Engineering, Shanghai Jiao Tong University, Shanghai 200240, China

ARTICLE INFO

Article history:
Received 5 September 2012
Received in revised form 8 March 2013
Accepted 8 March 2013
Available online xxx

Keywords:
Piezoceramic actuator
Hysteresis
Creep
Vibration
Motion control
Nanopositioning

ABSTRACT

In this paper, we develop a new integrated control strategy with creep, hysteresis and vibration compensation to achieve the high-performance motion control of piezoceramic actuators. For this purpose, the direct inverse compensation method is firstly applied to mitigate the asymmetric hysteresis nonlinearity without involving inverse model calculation. The hysteresis caused error is reduced by up to 81.35% to clearly verify the effectiveness of the proposed method. Then, a notch filter is designed to damp the vibrational dynamics of the compensated system, i.e., the plant with inverse hysteresis compensation, which increases the gain margin of the system from 5.4 dB to 21.7 dB. Finally, the feedback controller is developed to handle the creep nonlinearity, and modeling uncertainties of the system with hysteresis and vibration compensation. The developed integrated controller is demonstrated to improve the bandwidth of the piezo-actuated positioning system from 65 Hz to 605 Hz. With respect to variations of input frequencies, comparative experimental results are further presented to confirm the significantly better performances of the proposed control strategy in terms of speed and accuracy.

1. Introduction

In precision instruments such as micromanipulators [1,2], scanning probe microscopes [3] and atomic force microscopes [4,5], nanopositioning stages are becoming a promising technique to generate mechanical displacement with resolution down to the nanometer or sub-nanometer scale. The state-of-the-art nanopositioning stages generally utilize piezoceramic actuators for actuation due to their excellent advantages of high displacement resolution, fast response time and high stiffness [6]. However, the effects of creep, hysteresis, and vibration in piezoceramic actuators present a major challenge limiting the performances of piezo-actuated nanopositioning stages in terms of accuracy and speed. For example, creep is related to the drift effect of the output displacement with a constant applied voltage over extended periods of time [7], which becomes noticeable during slow-speed scanning operations. The hysteresis effect is the multi-valued nonlinear phenomenon between the applied voltage and the output displacement over relatively long-range displacements, which can produce positioning error up to 15% of the moving range at operating frequencies well below the first resonance frequency of piezoceramic actuators [6,8]. Vibration is a movement-induced oscillation effect, which leads to significant positioning errors when operating at high frequencies relative to the first resonance frequency of piezoceramic actuators. Typically, operating frequencies are restricted to less than 1/10th to 1/100th of the first resonance frequency, thus restricting the operating bandwidth of piezo-actuated nanopositioning systems [9,10].

To address such challenges, many efforts have been made in the literature to remedy these three adverse effects.

(i) For the creep compensation, several models such as the nonlinear logarithm model [7] and the linear dynamic model [11,12] have been developed to describe the creep effect. Then, an inversion of the creep model is constructed in a feedforward controller to compensate the creep. Rather than modeling the creep effect, the creep can also be mitigated by a feedback controller, for instance a proportional integral differential control law [13,14].

(ii) Owing to its non-smooth and non-memoryless nature as well as multi-valuedness, the hysteresis effect is a major disadvantage to cause severe limitations on the high-accuracy performance of piezo-actuated nanopositioning stages [15,16]. The existing control techniques for hysteresis compensation can be roughly classified into three categories: charge control, feedforward control, and feedback control. Charge control [17] in comparison with voltage control is an effective approach to reduce the hysteresis effect based on the fact that there is a less hysteresis nonlinearity between the displacement

* Corresponding author. Tel.: +86 21 34206545; fax: +86 21 34206086.
E-mail addresses: guguoying@sjtu.edu.cn (G.-Y. Gu), zhulm@sjtu.edu.cn (L.-M. Zhu).

0924-4247/$ – see front matter © 2013 Elsevier B.V. All rights reserved.
http://dx.doi.org/10.1016/j.sna.2013.03.005

of a piezoceramic actuator and the applied charge than the one between displacement and applied voltage. However, this technique generally leads to the complex implementation and expensive cost of the charge amplifier [6] and leads to further reduction of the travel range and the positioning bandwidth of piezoceramic actuators [18]. In the voltage control case, feedforward control is the most common control technique to mitigate the nonlinear hysteresis effect. The main idea of the feedforward hysteresis compensation is to develop a mathematical model that describes the hysteresis nonlinearity, and then to construct an inverse model based feedforward controller to linearize the actuator response [19,20]. It refers, in particular, to the utilization of a hysteresis model accurately describing the hysteresis nonlinearity. Various models have been developed for this purpose, for example, the Bouc-Wen model [21], the polynomial approximation model [14], the Preisach model [22–25], the Prandtl–Ishlinskii model [26–30], frequency domain characterization [31], etc. However, due to the modeling errors and plant uncertainties, the feedforward controller cannot correct for the tracking errors [6]. Therefore, feedback control is usually integrated with the feedforward controller to improve the tracking performance of piezoceramic actuators, which was pioneered by Ge and Jouaneh [8]. The reader may also refer to [10,14,32,33] for a recent review of the combined feedforward-feedback control strategy for piezoceramic actuators. As an alternative, some attempts [15,34–37] have also been made to fuse the hysteresis models with robust control approaches to mitigate the hysteresis effect without the inverse hysteresis construction.

(iii) The vibration effect due to the mechanical oscillation is the main factor limiting the high-speed performance of the piezo-actuated nanopositioning stages [10]. One way to increase the required speed is to build a piezo-actuated stage that is sufficiently stiff and small [38]. A disadvantage of this approach is that its maximum traversal range is limited to a few microns. In addition, the tracking bandwidth is still limited by the resonant frequency of the piezoceramic actuators. Therefore, development of control techniques to suppress the vibration effect becomes popular. As reported in the literature, the effective method to damp the resonant modes is the utilization of vibration controllers such as the notch filters [5,39], integral resonant controllers [40], input shaping controllers [4,12] and model-based feedforward controllers [11]. It is worthy of mentioning that before these vibration controllers are developed for the piezo-actuated nanopositioning stage, the hysteresis nonlinearity should be sufficiently eliminated in advance.

As can be seen from above, development of control techniques to mitigate the creep, hysteresis and vibration effects of piezoceramic actuators has attracted significant interests and attentions. However, till now the integrated compensation controllers for these three adverse effects are still scarce. As far as we know, only two groups have reported the integrated works. Prof. Devasia's group at University of Washington [11] first developed an integrated controller for the creep, hysteresis and vibration compensation, where the creep was compensated by the inverse of a linear dynamic creep model, the hysteresis was linearized by the inverse Preisach model, and the vibration was suppressed by using the inversion of vibrational dynamics. Without using the Preisach model and model-based feedforward controller, Rakotondrabe et al. [12] presented an extensive work, where an inverse of the Prandtl–Ishlinskii model was used to cancel the hysteresis effect and an input shaping technique was adopted to compensate for the vibration. Based on these accumulated results [11,12,41], this paper proposes a new integrated controller to compensate for the creep, hysteresis and vibration effects, and comparative experimental results are presented to demonstrate the performance enhancement of the proposed controller in terms of speed and accuracy. The novelty and main contributions of this paper presented lie on that: (1) the direct inverse compensation method with a modified Prandtl–Ishlinskii model is applied to mitigate the asymmetric hysteresis nonlinearity without involving inverse model calculation; (2) a notch filter is implemented to damp the vibration effect of the plant with hysteresis compensation; (3) a feedback controller is finally designed to handle the creep nonlinearity, and modeling uncertainties of the system with hysteresis and vibration compensation.

The remainder of this paper is organized as follows. In the next section, the experimental setup is presented. In Section 3, the direct inverse compensation method is applied to mitigate the hysteresis nonlinearity. In Section 4, the vibration compensation is detailed. After that, the high-gain feedback controller is designed to achieve the high-performance motion control in Section 5, followed by the conclusion in Section 6.

2. Experimental setup

The experimental setup is shown in Fig. 1. Fig. 1(a) depicts the experimental platform, which consists of a piezo-actuated stage, a dSPACE DS1103 board equipped with the 16-bit DAC and 16-bit ADC, a piezo amplifier, and a signal conditioner. The piezo-actuated stage is composed of an one-dimensional monolithic flexure mechanism, a piezoceramic actuator (PCA), and a strain gauge sensor (SGS). The structure and working principle of the piezo-actuated one-dimensional monolithic flexure mechanism is illustrated in Fig. 1(b), where the double parallelogram flexure is adopted to remove the parasitic motions. The PCA is a preloaded piezoelectric stack actuator (PSt 150/7/100 VS12 from Piezomechanik in Germany), which is used to drive the flexure mechanism with the nominal 75 μm displacement. The high-resolution SGS integrated into the PCA is adopted to measure the real-time position of the PCA through the variance of the electrical resistance. The output signals of the SGS pass through the signal conditioner and are simultaneously captured by the 16-bit ADC for the dSPACE controller. The dSPACE DS1103 board (from dSPACE in Germany) is employed to implement the developed control algorithms in the Matlab/Simulink environment. The DAC board produces an analog voltage output for the piezo amplifier, which is then amplified by 15 times to drive the PCA with excitation voltage ranging from 0 to 150 V. As discussed above, the block diagram of the experiment setup is intuitively shown in Fig. 1(c). In the following development, the proposed controller for hysteresis, creep and vibration compensation will be addressed in detail.

Remark: It is worthy of mentioning that the piezo-actuated stage used in this work is a one-dimensional monolithic flexure mechanism. The flexure mechanism has the advantages of no friction, no backlash, no wear, and compact structure. In addition, there is no coupling effect caused by different motion directions due to the one-dimensional characteristics of the flexure mechanism. In this case, the strain gauge sensor is utilized as the displacement sensor in this work and the extension of the piezoelectric actuator can be approximately recognized as the displacement of the end effector. In order to directly measure the displacement of the end effector, external displacement sensors such as capacitive sensors or LVDT sensors are required.

3. Modified P–I model based inverse hysteresis compensation

The hysteresis of the piezoceramic actuator is an inherent multi-valued nonlinearity with the asymmetric characteristic,

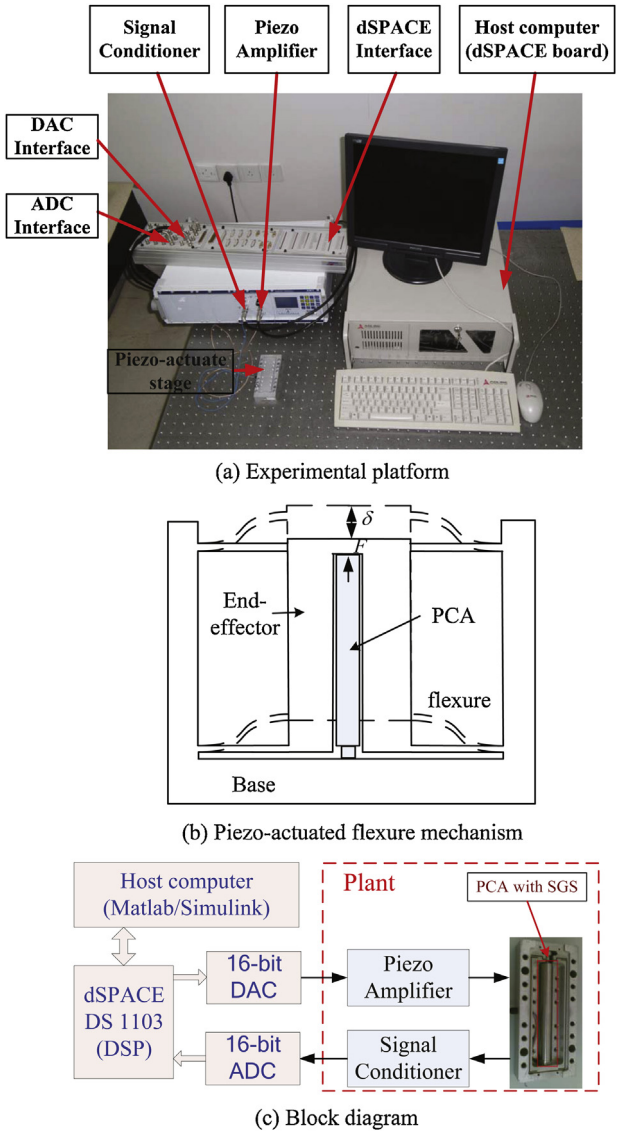

Fig. 1. The experimental setup for controlling the piezo-actuated nanopositioning stage.

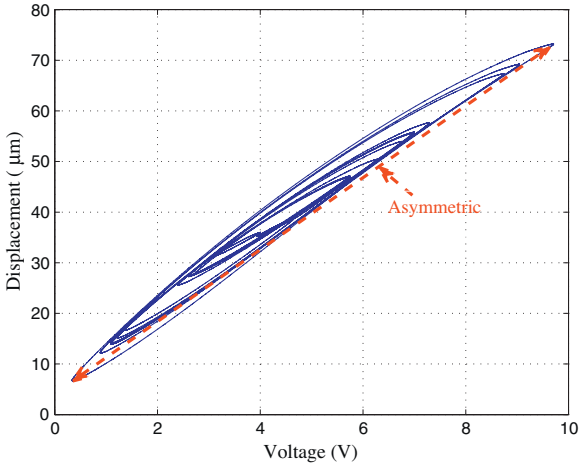

Fig. 2. The hysteresis nonlinearity of the piezoceramic actuator.

which can be observed in the relationship between the applied voltage and corresponding displacement of the piezoceramic actuator as shown in Fig. 2. Recent studies [42–45] show that the hysteresis in the piezoceramic actuator presents dynamic or rate-dependent behavior as well. In the reported previous works [15,46], the rate-dependent behavior can be well represented by a linear dynamic plant preceded by a rate-independent hysteresis model. In this section, we shall mitigate the asymmetric the hysteresis nonlinearity using a real-time direct inverse compensation method [41] with a rate-independent hysteresis model.

Different from the commonly used procedures, the new concept of the direct inverse hysteresis compensation is motivated by the fact that the inversion of the hysteresis nonlinearity is by nature hysteresis loops. The difference between the inverse hysteresis and the real hysteresis in piezoelectric actuator is the orientation of the hysteresis loops. From the mathematical point of view, an available hysteresis model can be directly applied to characterize the inverse hysteresis effect instead of modeling the real hysteresis nonlinearity. Subsequently, the identified hysteresis model can be directly cascaded in the feedforward path for hysteresis cancelation, which thus avoids the complex and difficult mathematical calculation for developing an inversion of the identified hysteresis model. With the hysteresis compensation, the resulting system can be considered as a quasi linear plant, making it easy for the development of a linear vibration controller to damp the vibration effect.

3.1. Direct inverse hysteresis compensation

The direct inverse hysteresis compensation method is applied in this work to linearize the asymmetric hysteresis nonlinearity by directly modeling the inverse hysteresis effect through a hysteresis model. It refers to the utilization of a hysteresis model accurately describing the inverse hysteresis effect. Considering the asymmetric hysteresis characteristic of the piezoceramic actuator as shown in Fig. 2, the classical Prandtl–Ishlinskii (P–I) model [26] original for the symmetric hysteresis description is insufficient. The modified P–I model defined in terms of weighted play operators and a polynomial input function is defined as [41]

$$y(t) = h(x(t)) + \int_0^R p(r)F_r[x](t)dr \tag{1}$$

where $x(t)$ is the input, $y(t)$ is the output, $h(x(t)) = a_1x^3(t) + a_2x(t)$ is a polynomial input function with constant a_1 and a_2, $p(r)$ is a density function that is generally calculated from the experimental data. Considering the positive excitation nature of the used piezoceramic actuator, the one-side play operator $F_r[x](t)$ [26,41] is adopted in this work, whose transfer characteristic is shown in Fig. 3. It should be noted that the difference between the modified P–I model (1) and the classical P–I model is the selection of the input function $h(x(t))$. The benefit for choosing such input function is that the modified P–I model can describe the real hysteresis loops in the piezoceramic actuators with asymmetric behaviors. The reader may refer to [41] for a detailed discussion.

To compensate for the hysteresis, the modified P–I model is firstly identified through the experimental data of the inverse hysteresis effect. Then, the feedforward controller with the identified hysteresis model is cascaded in the feedforward path to linearize the real hysteresis nonlinearity of the piezoceramic actuator. As an illustration, Fig. 4 shows the principle of the direct inverse hysteresis compensation method.

In order to develop the feedforward controller in practice, the compensation signal $v_h(t)$ is obtained by a discrete form of the

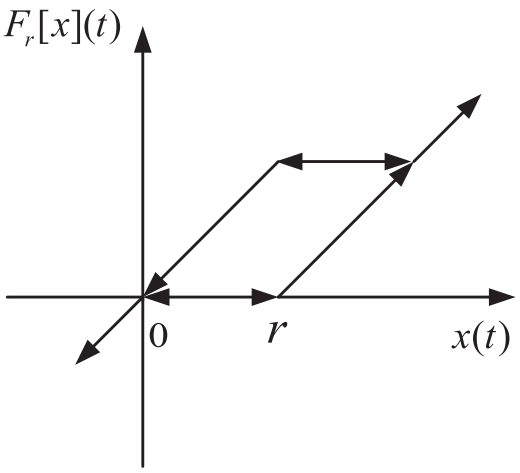

Fig. 3. Input–output relationship of the one-side play operator.

modified P–I model (1) with a finite number of play operators rather than with an infinite number of play operators as follows:

$$v_h(t) = g(y_h(t)) + \sum_{i=1}^{n} b(r_i) F_{r_i}[y_h](t) \tag{2}$$

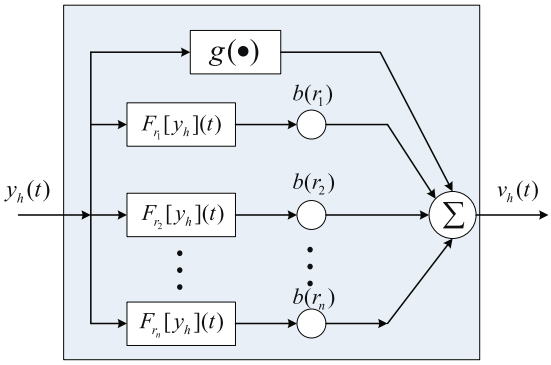

Fig. 5. Block diagram of the numerical implementation for the feedforward controller (2).

where $y_h(t)$ is the referenced trajectory, $g(y_h(t)) = p_1 y_h^3(t) + p_2 y_h(t)$, n is the number of the adopted play operators for modeling, and $b(r_i) = p(r_i)(r_i - r_{i-1})$ are the weighted constant for the threshold r_i. Fig. 5 shows the block diagram for implementation of the feedforward controller (2).

3.2. Experiments

Before implementing the controller (2) for experimental validation, the parameters n, r_i, p_1, p_2 and $b(r_i)$ should be obtained. In

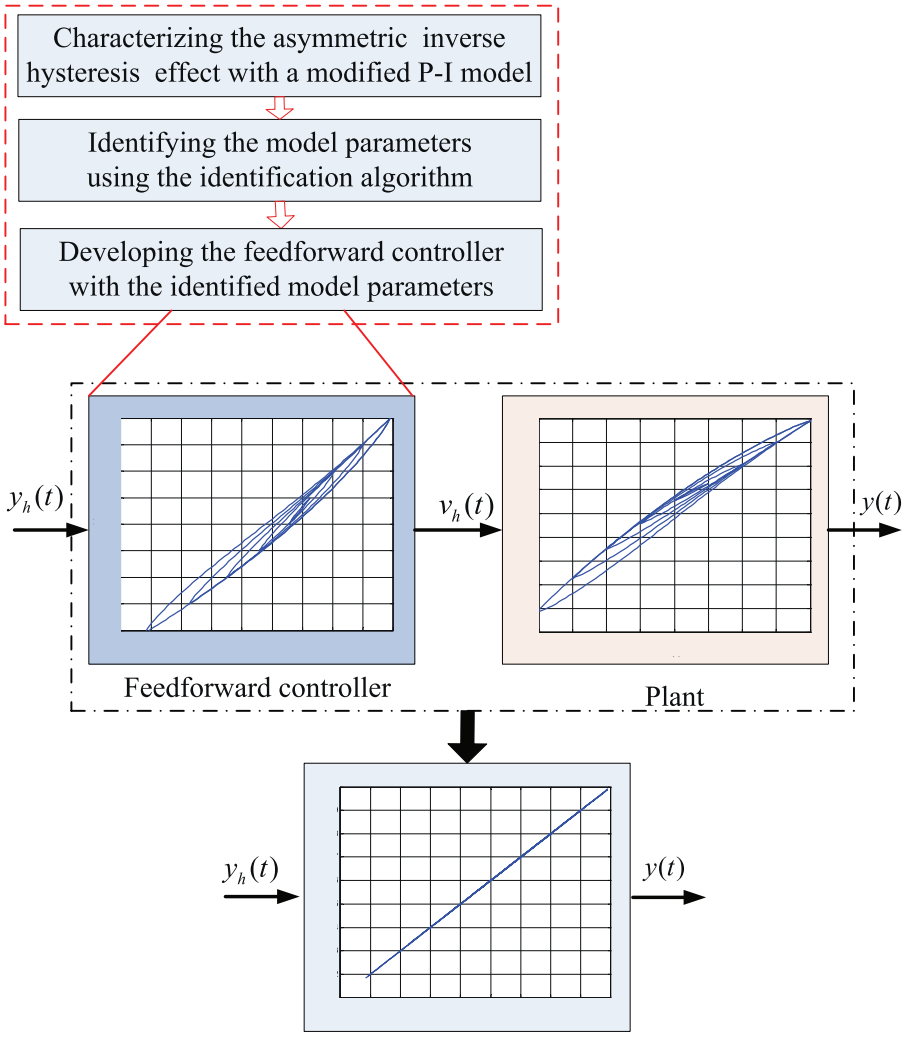

Fig. 4. Principle of the direct inverse hysteresis compensation method.

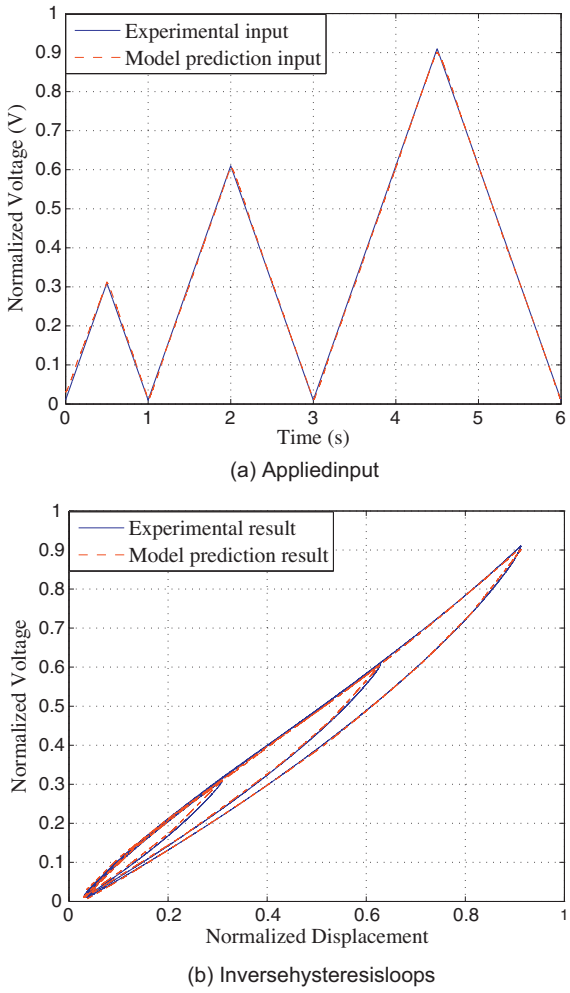

Fig. 6. Comparison of the modified P–I model prediction results and experimental results. (a) Applied input and (b) inverse hysteresis loops.

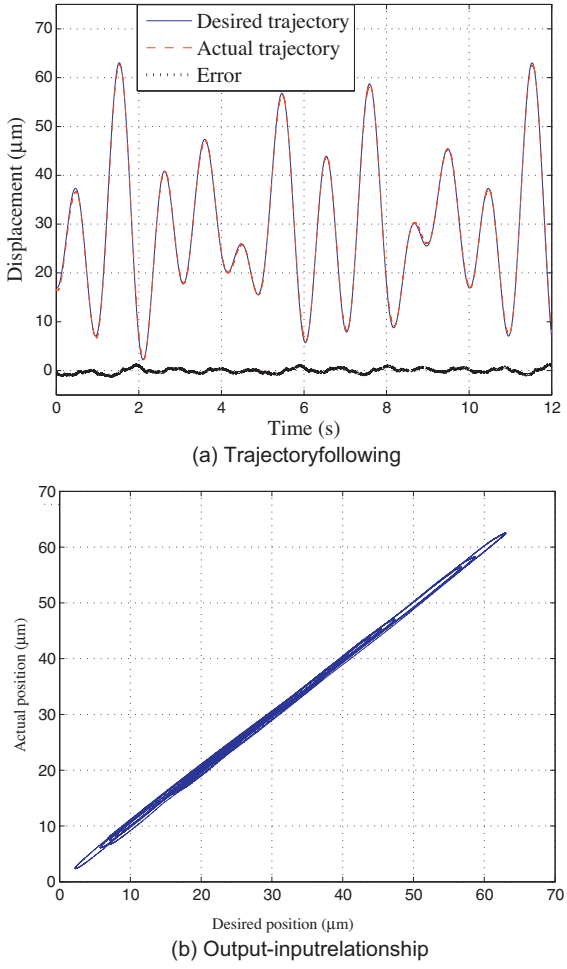

Fig. 7. Feedforward experimental results with inverse hysteresis compensation. (a) Trajectory following and (b) output–input relationship.

this work, ten play operators (i.e. $n = 10$) are chosen for parameters identification and hysteresis compensation with fixed threshold values r_i defined as

$$r_i = \frac{i}{n}||y_h(t)||_\infty, \quad i = 0, 1, 2, \ldots, n-1 \tag{3}$$

with $||y_d(t)||_\infty = 1$ in the normalized case. Then, the particle swarm optimization algorithm [41,47] is used to identify other parameters p_1, p_2 and $b(r_i)$ with experimental data. Following the design steps of the direct inverse hysteresis compensation method in Fig. 4, a triangular input voltage (indicated by the blue solid line in Fig. 6(a)) was first applied to excite the piezoceramic actuator, and experimental data are used to identify the parameters. The prediction results of the identified model verified with the experimental results are compared in Fig. 6. The standard deviation of the error σ_h in the predicted response is

$$\sigma_h = \frac{\sqrt{1/(N-1)\sum_{i=1}^{N}(v_{hi} - v_{hi}^p)^2}}{\max_i(v_{hi}) - \min_i(v_{hi})} \times 100\% = 0.55\%, \tag{4}$$

and the maximum error e_{maxh} is

$$e_{maxh} = \frac{\max_i(v_{hi} - v_{hi}^p)}{\max_i(v_{hi}) - \min_i(v_{hi})} \times 100\% = 1.29\%, \tag{5}$$

where v_{hi} is the actual applied voltage, v_{hi}^p is the predicted applied-voltage obtained by using the modified P–I hysteresis model, and N is the number of experimental data points for identification.

With the identified hysteresis model, the feedforward controller (2) as shown in Fig. 5 was then implemented to cancel the hysteresis nonlinearity. Fig. 7 shows the feedforward experimental results with the referenced multi-amplitude signal. The maximum tracking error with the hysteresis compensation is about 1.24 μm. As a contrast, Fig. 8 shows the open-loop experimental results without inverse hysteresis compensation, where the asymmetric hysteresis is clearly observed and the maximum error of the open-loop system is about 6.47 μm. From Fig. 8, we obtain that the maximum hysteresis caused error is about $e_{mhe} = 13.19\%$, defined as

$$e_{mhe} = max\left|\frac{MHE}{\max(y_h) - \min(y_h)}\right| \times 100\%. \tag{6}$$

When the feedforward controller for hysteresis compensation is utilized, the maximum hysteresis caused error as described in Fig. 7(b) is about $e_{mhe} = 2.46\%$, which is reduced by up to 81.35% comparing with the open-loop result as shown in Fig. 8. From Fig. 7(b), it can also be seen that the hysteresis nonlinearity is greatly mitigated with direct inverse compensation and the resulted relationship between the desired position and the actual position is almost linear and symmetric. It clearly demonstrates the effectiveness of proposed method for asymmetric hysteresis compensation. In the following development, a notch filter will be

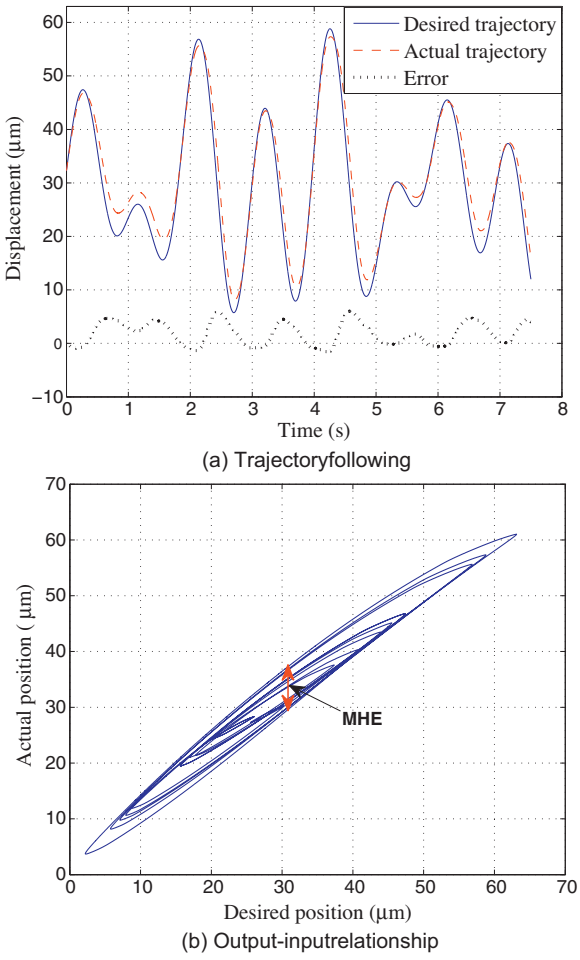

Fig. 8. Open-loop experimental results without hysteresis compensation. (a) Trajectory following and (b) output–input relationship.

designed for the compensated plant with hysteresis compensation to suppress the vibration effect.

Remark: It should be noted that the purpose of Figs. 7 and 8 is to show stable tracking results of the developed controllers, where the transient period is not included since it does not influence the analysis. However, it is generally difficult to determine the exact time of the presented data, if not impossible. For simplicity, relative notions for the time labels starting from 0 are used in these figures as usually treated in the literature.

4. Notch filter for vibration compensation

In this section, we describe and damp the vibrational dynamics of the compensated system, i.e., the plant with inverse hysteresis compensation as shown in Fig. 9. As reported in the literature, the linear system based control techniques such as the notch filters [5,39], integral resonant controllers [40], input shaping controllers [4,12] and model-based feedforward controllers [10,11] can be used to suppress the unwanted vibration mode of piezoceramic actuators. In this work, the notch filter is adopted to damp the vibration dynamics.

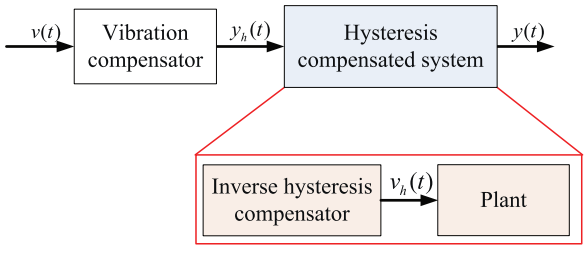

Fig. 9. Block diagram of the new system with hysteresis compensation.

4.1. Principle of the notch filter

The notch filter is a band-stop filter with a narrow stopband, thus making it convenient and effective for eliminating the sharp resonance with a signal peak in the frequency response [5,39]. It is generally used to improve the high-bandwidth performance of high-gain feedback controllers.

The transfer function $N_f(s)(s = i\omega)$ of a standard second-order notch filter is given by

$$N_f(s) = \frac{s^2 + 2\zeta_1\omega_0 s + {\omega_0}^2}{s^2 + 2\zeta_2\omega_0 s + {\omega_0}^2}, \tag{7}$$

where $\omega_0 = 2\pi f_0$ is the center frequency with the resonance peak f_0, ζ_1 and ζ_2 are the damping factors. It is noted that when $s = i\omega_0$, $N_f(s)$ becomes ζ_1/ζ_2 without phase change, which gives the minimum transmission rate [5].

In practice, the values ω_0 and ζ_1 are selected according to the vibrational dynamics of the controlled system, while ζ_2 is generally set to 1 for simplicity. For example, to suppress the resonance of the plant characterized by a simple transfer function ${\omega_1}^2/(s^2 + 2\zeta\omega_1 s + {\omega_1}^2)$, ω_0 and ζ_1 in (7) should be tuned to ω_1 and ζ separatively. Using $\zeta_2 = 1$, the composite transfer function with the notch filter (7) becomes ${\omega_1}^2/(s^2 + 2\omega_1 s + {\omega_1}^2)$. As a result, the vibration effect of the plant are completely damped.

4.2. Experiments

As the above discussions, the vibrational dynamics model of the hysteresis compensated system as shown in Fig. 9 should be firstly identified in order to design the notch filter for vibration compensation. For this purpose, a band-limited white noise signal is used to excite the hysteresis compensated system. The system identification toolbox of MATLAB is then adopted to obtain the frequency response in the Laplace domain relating the input y_h to

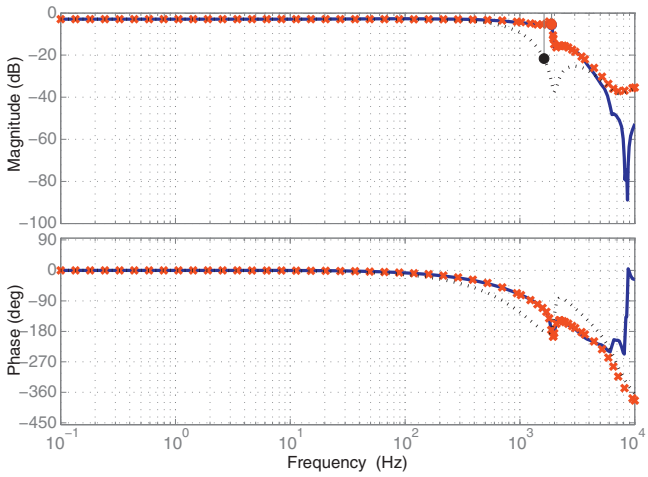

Fig. 10. Comparison of frequency responses: blue solid line-experimental response; red star line-model prediction response; black dotted line-model prediction response with the notch filter. (For interpretation of the references to color in this figure legend, the reader is referred to the web version of the article.)

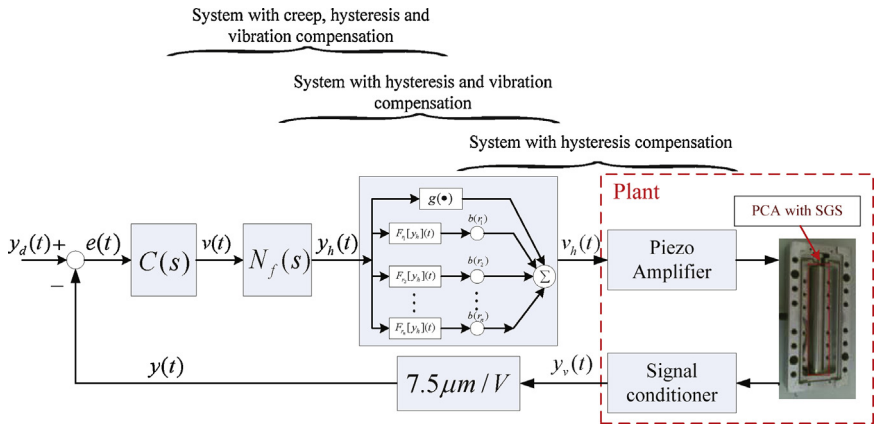

Fig. 11. Block diagram of the complete system with the creep, hysteresis and vibration compensation.

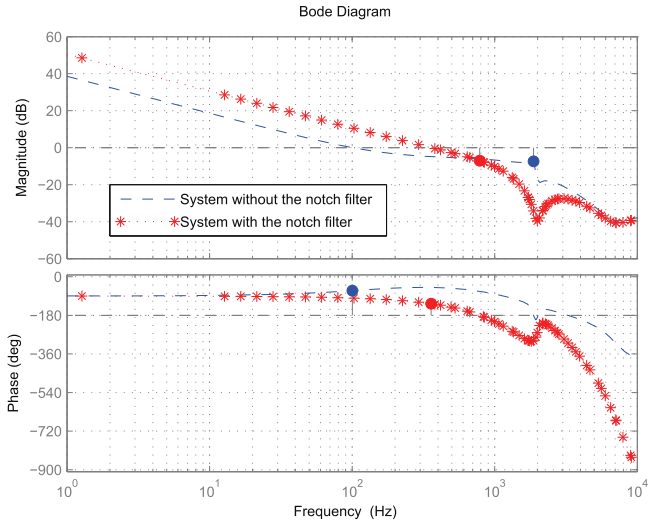

(a) Open-loop system

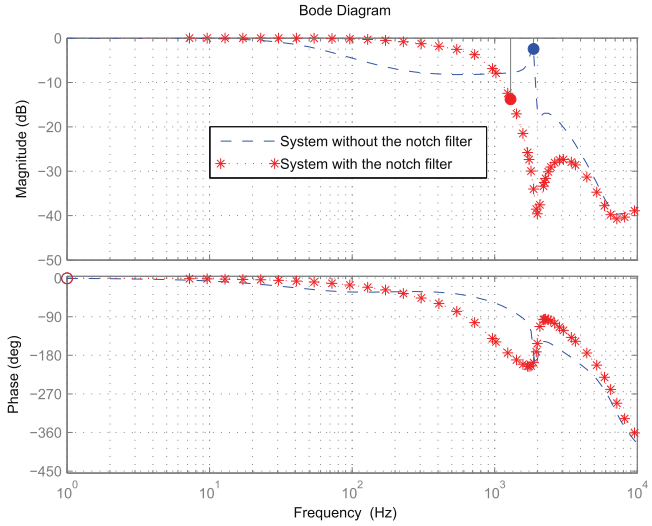

(b) Closed-loop system

Fig. 12. Comparison of the frequency responses of the system with and without the notch filter. (a) Open-loop system and (b) closed-loop system.

the sensor output y_v of the piezoceramic actuator. The identified linear dynamic model is represented as

$$\widehat{G}_f(s) = k_0 \frac{\prod_{m=1}^{5}(s - z_m)}{\prod_{n=1}^{5}(s - p_n)} \left(\frac{V}{\overline{V}}\right) \tag{8}$$

where $k_0 = -0.017996$ is the nominal gain factor, the zeros (z_m, for $m = 1, 2, \ldots, 5$) are 121400, $10555 \pm i4222$ and $-547.5 \pm i12510$ (unit rad/s), and the poles (p_n, for $n = 1, 2, \ldots, 5$) are -62080, $-8500 \pm i5749$ and $-502.5 \pm i11792$ (unit rad/s). It is noted that the unit of the transfer function $G_f(s)$ can be expressed in the actual displacement unit (μm/V) by multiplying $\widehat{G}_f(s)$ with the static sensor gain 7.5 μm/V, i.e., $G_f(s) = 7.5\widehat{G}_f(s)$ μm/V. To verify the identified model (8), Fig. 10 shows the comparison of the model prediction frequency response (indicated by the red star line) and the experimental response (indicated by the blue solid line). It is observed that the identified model reasonably well follows the resonant dynamics of the measured system up to 3.5 kHz.

With the identified model (8), it is ready to design the notch filter (7) for vibration compensation. Analyzing the dynamics characteristics of the identified model (8), there are two very close resonance peaks at 1633 Hz and 1878 Hz, and the damping factors at these two resonance peaks are 0.8283 and 0.0426

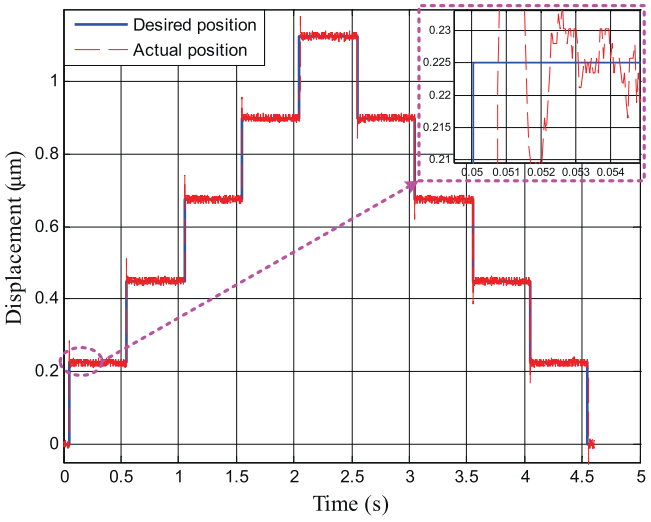

Fig. 13. Experimental results of the feedback controller with the step-like trajectory.

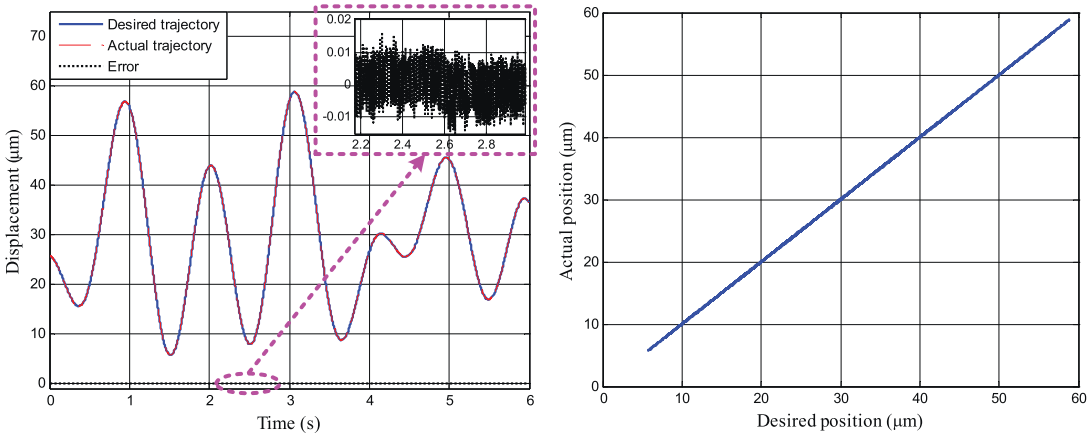

(a) Trajectory tracking (b) Output-input relationship

Fig. 14. Experimental results of the feedback controller with the multi-amplitude trajectory. (a) Trajectory tracking and (b) output–input relationship.

respectively. Therefore, the notch filter is designed to suppress the second resonance peak with the low damping factor at 1878 Hz as follows:

$$N_f(s) = \frac{s^2 + 1005s + (1878 \times 2\pi)^2}{s^2 + 23,115s + (1878 \times 2\pi)^2}. \quad (9)$$

In this work, the notch filter (9) was realized in the Matlab software using the dSPACE rapid prototyping control system. The resulted frequency response with the notch filter is shown by the black dotted line in Fig. 10, together with the experimental frequency response of the original system without the notch filter for comparing the old and new gain margins. It can be seen from Fig. 10 that the frequency response of the composite system with the notch filter shows significant increase in the gain margin from 5.4 dB to 21.7 dB. Moreover, it is known that the feedback controller gains are limited by the low gain margin imposed by the low damped mechanical resonance. Due to the introduction of the notch filter, the gain margin is evidently increased. Hence, the maximum bandwidth of the feedback controller that is inversely proportional to the magnitude of the resonant peak [40] can be achieved. Therefore, it is ready to design the high-gain feedback controller in the following development.

5. Feedback controller

The foremost control objective of the piezoceramic actuator is to minimize tracking errors caused by the creep, hysteresis and vibration effects. In the aforementioned sections, we have addressed related compensation methods for the hysteresis and vibration effects. In this section, a feedback controller with higher control gains is designed to compensate the creep, and modeling uncertainties for the new system with hysteresis and vibration compensation as shown in Fig. 11.

5.1. Controller design

As shown in Fig. 11, the feedback control system is comprised of the set-point summing junction, the controller $C(s)$ and the new system $G_n(s) = 7.5N_f(s)\widehat{G}_f(s)$, i.e. the plant with hysteresis and vibration compensation. Generally, the challenge with designing a feedback controller for the piezo actuated system is the low gain margin problem inherent in this system [10,18]. As addressed in Section 4, the notch filter has been developed in this work

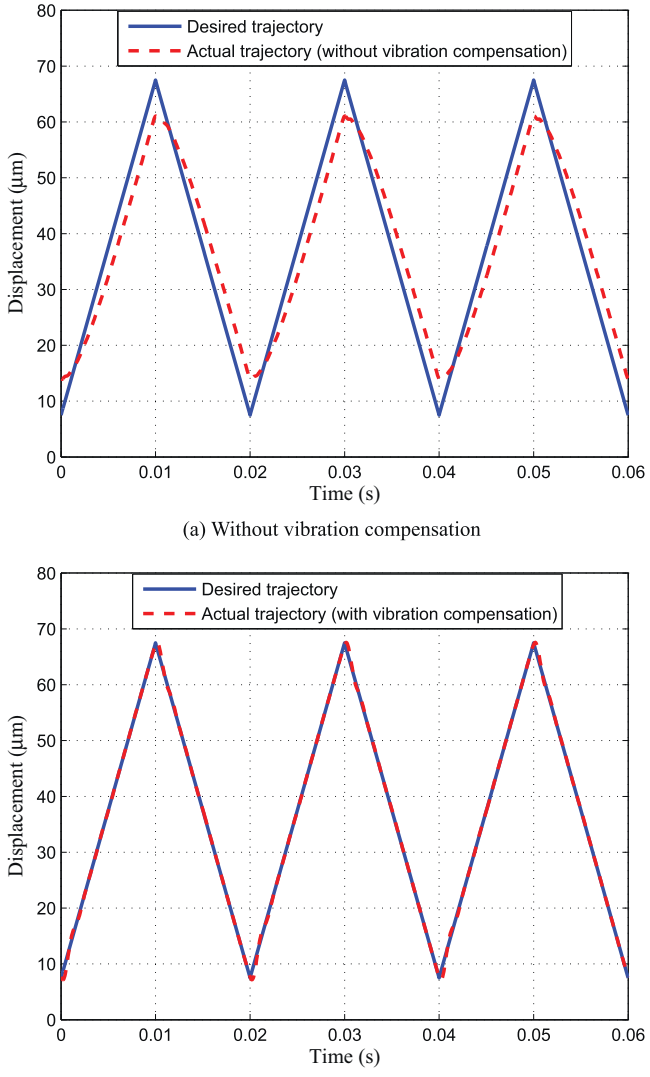

(a) Without vibration compensation

(b) With vibration compensation

Fig. 15. Comparison of the performance of the closed system with and without vibration compensation for a 50 Hz triangular reference. (a) Without vibration compensation and (b) with vibration compensation. (For interpretation of the references to color in the text, the reader is referred to the web version of the article.)

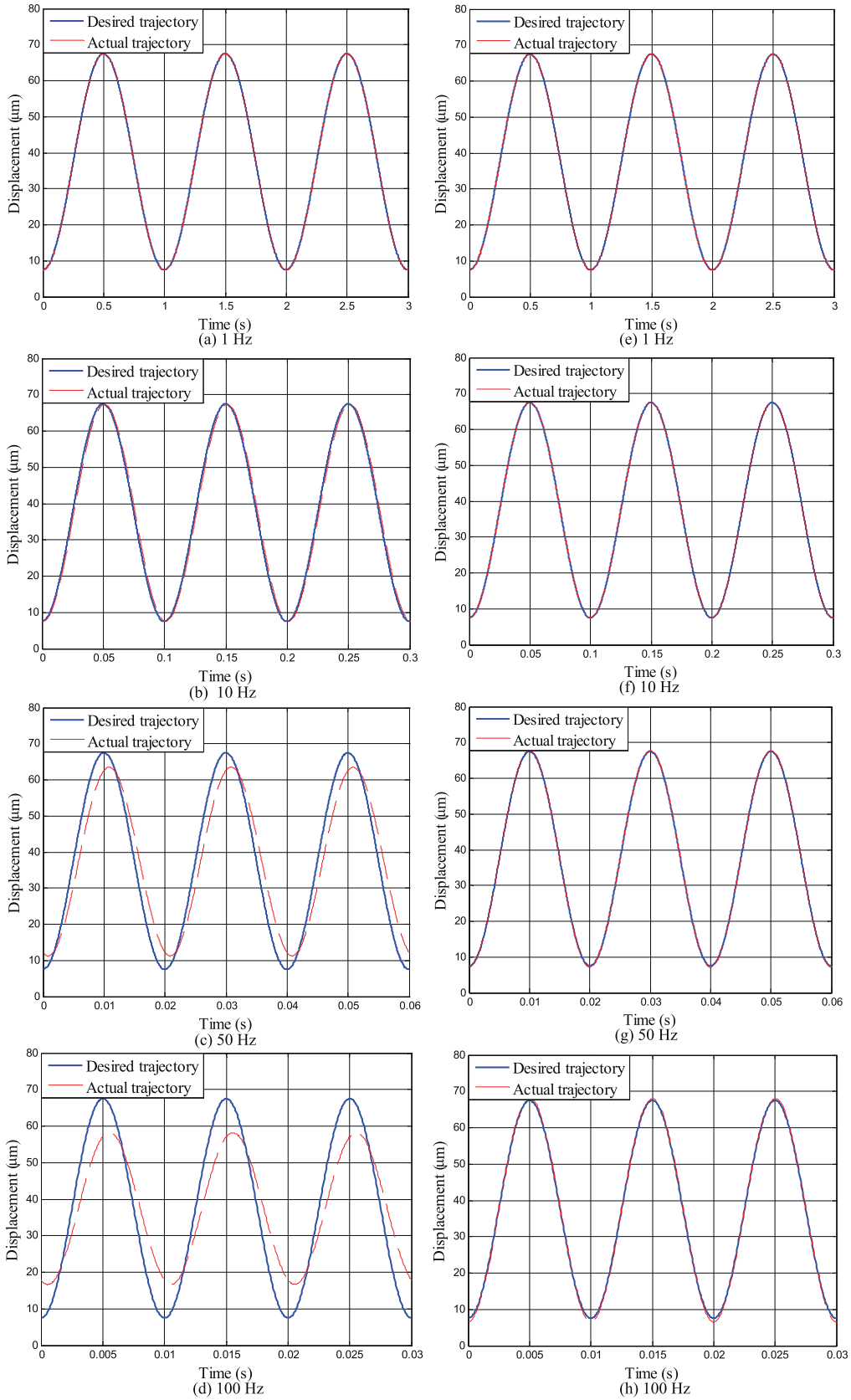

Fig. 16. Comparisons of the feedback controllers with and without vibration compensation under various references: (a)–(d) PI controller without vibration compensation and (e)–(h) high-gain PI controller with vibration compensation.

Table 1
Performances of the feedback controller with and without the notch filter (NF).

Items	Without NF	With NF
$C(s)$	$0.1+100/s$	$0.1+400/s$
Gain margin	7.34	7.02
Phase margin	115°	54°
Bandwidth	67 Hz	605 Hz

to increase the gain margin of the system from 5.4 dB to 21.7 dB (shown in Fig. 10), which enables the use of the feedback controller with higher control gains.

To develop the controller $C(s)$, various control approaches, such as, proportional-integral-derivative control [8,13,32], sliding model control [35,37], and robust adaptive control [15,34,36] have been proposed. Among these options, the most popular choice for compensation in commercial scanning probe microscopes (SPMs) or atomic force microscopes (AFMs) is the integral controller or proportional-integral (PI) controller [17,18,39] because of the advantages of simple implementation and robust to modeling errors. Without losing generality, the PI controller is developed in this work for the following illustration.

The PI controller in the continuous time domain is described by the following:

$$v(t) = k_p e(t) + k_i \int_0^t e(\tau)d\tau \tag{10}$$

where k_p and k_i are the proportional gain and integral gain respectively, $e(t) = y_d(t) - y(t)$ is the tracking error between the actual position $y(t)$ and desired position $y_d(t)$. Moreover, the transfer function of the controller $C(s)$ is given

$$C(s) = \frac{k_p s + k_i}{s}. \tag{11}$$

Analyzing the root-locus plot of the open loop system $G_f(s)$, we obtain that the closed loop system $(CG_f)/(1+CG_f)$ without the notch filter will be unstable if feedback gains are greater than 0.2479. Hence, the gain k_p in the case of the proportional controller should satisfy $0 < k_p < 0.2479$. As is evident in [18], a trade-off between robustness and performance has to be determined for the controller $C(s)$ with a PI structure by tuning the parameters k_p and k_i. In this work, we choose $k_p = 0.1$ and $k_i = 100$ to guarantee a gain margin of about 7.34 dB and a phase margin of 115° (as shown in Fig. 12(a)) and the corresponding −3 dB bandwidth of the closed loop system $(CG_f)/(1+CG_f)$ without the notch filter is about 67 Hz (as shown in Fig. 12(b)). When the notch filter is introduced, the gain k_i can evidently increase to achieve the higher control bandwidth. Therefore, the controller $C(s)$ with a large integral gain $k_i = 400$ can be applied while maintaining a gain-margin of 7.02 dB. As an illustration, Fig. 12 shows the comparison of the frequency responses of the open-loop system and closed-loop system with and without the notch filter, where $k_i = 400$ for the case with the notch filter. It can be observed that the phase margin of the system with the notch filter is 54° and the corresponding control bandwidth is about 605 Hz, which is increased by about 9 times in comparison with the one, i.e. 67 Hz, in the no notch filter case. In summary, performances of the feedback controller with and without the notch filter (NF) are listed in Table 1.

5.2. Experiments

The developed PI feedback controller with the inverse hysteresis compensator and the notch filter was implemented on the piezo-actuated nanopositioning stage discussed in Section 2. The experimental results are shown in Figs. 13 and 14. Fig. 13 shows the experimental results with the step-like trajectory. From this figure, we can observe that the rising time is about 0.7 ms and the stage response converges to each new set-point within a 5% error band after about 2 ms with no steady-state error. Fig. 14 shows the experimental results with the desired multi-amplitude trajectory, where the maximum hysteresis caused error is $e_{mhe} = 0.068\%$, and the root-mean-square (RMS) tracking error is $e_{rms} = 0.0072\%$, defined as

$$e_{rms} = \frac{\sqrt{(1/T)\int_0^T (y(t) - y_d(t))^2 dt}}{\max(y_d(t)) - \min(y_d(t))} \times 100\%. \tag{12}$$

Table 2
RMS tracking errors e_{rms} of the sinusoidal tracking performance of feedback controllers with and without vibration compensation (VC).

VC	1 Hz	10 Hz	50 Hz	100 Hz
Without	0.23%	2.34%	10.07%	14.57%
With	0.0071%	0.040%	0.32%	0.93%

In comparison to the feedforward experimental results as shown in Fig. 7, the PI controller with the vibration compensation greatly reduces the tracking errors by approximately two order of magnitude, which demonstrates the high-accuracy performance of the developed controller.

To evaluate the performance of the closed loop system at high speeds, a triangular wave with the fundamental frequency of 50 Hz was adopted for tracking. Fig. 15 shows a comparison of the tracking performance of the closed systems with and without vibration compensation. The blue solid lines indicate the desired position, while the red dashed lines represent the actual position. From this figure, it can be seen that the high-speed performance of the designed high-gain feedback controller is significantly better than the controller without the notch filter. In order to further elucidate the high-bandwidth advantage of the high-gain feedback controller, Fig. 16 also shows comparisons of the experimental results with the desired and actual position for 1, 10, 50 and 100 Hz sinusoidal reference signals. In addition, the RMS tracking errors corresponding to the moving range (i.e. 60 μm) are listed in Table 2. It is worthy of mentioning that due to its lower bandwidth of 67 Hz the RMS errors of the closed system without vibration compensation increase substantially by increasing the scan frequencies. With the introduction of the notch filter, the high-gain PI controller is designed to achieve substantial improvement in bandwidth of 605 Hz. In the closed system with vibration compensation, the RMS errors for all closed loop scans with different frequencies remain below 1%, which are much smaller than that of the closed system without vibration compensation. In particular, for the 100 Hz scan, the proposed controller reduces the RMS error by 93.62% (from 14.57% to 0.93%). Therefore, we can conclude that the proposed control strategy for piezoceramic actuators achieves significantly better tracking performance in terms of speed and accuracy.

6. Conclusion

This paper presents a new integrated controller to compensate for the creep, hysteresis and vibration effects of the piezoceramic actuator with experimental validations. Several distinct features of this paper are summarized as follows.

(1) Different from the commonly used inverse hysteresis compensation, the direct inverse compensation method with a modified Prandtl–Ishlinskii model is firstly proposed to mitigate the asymmetric hysteresis nonlinearity without involving inverse model calculation. The asymmetric hysteresis caused error is reduced by up to 81.35% to clearly verify the effectiveness of the proposed method.

(2) For the hysteresis compensated system (i.e. the plant with direct inverse hysteresis compensation), a band-limited white noise signal is applied to identify model parameters using the system identification toolbox of MATLAB. A notch filter is then designed to increase the gain margin from 5.4 dB to 21.7 dB by damping the vibration effect of the hysteresis compensated system.
(3) A PI feedback controller with high control gains is finally designed to handle the creep nonlinearity, and modeling uncertainties of the plant with hysteresis and vibration compensation. With the developed controller, the bandwidth of the piezo-actuated positioning system is significantly increased from 65 Hz to 605 Hz. Furthermore, comparative experimental results are presented to demonstrate the better performances of the proposed control strategy in terms of speed and accuracy.

Acknowledgements

The authors would like to thank Professor Chun-Yi Su at Concordia University, Canada for his valuable discussions and suggestions. This work was supported by the National Natural Science Foundation of China under Grant No. 91023047, and the Science and Technology Commission of Shanghai Municipality under Grant No. 11520701500 and the "Shu Guang" Project of Shanghai Municipal Education Commission under Grant No. 10SG17, and Shanghai Postdoctoral Scientific Program under Grant No. 13R21414000.

References

[1] B.J. Kenton, K.K. Leang, Design and control of a three-axis serial-kinematic high-bandwidth nanopositioner, IEEE/ASME Transactions on Mechatronics 17 (2) (2012) 356–369.
[2] M.N.M. Zubir, B. Shirinzadeh, Y. Tian, Development of a novel flexure-based microgripper for high precision micro-object manipulation, Sensors and Actuators A: Physical 150 (2) (2009) 257–266.
[3] S.M. Salapaka, M.V. Salapaka, Scanning probe microscopy, IEEE Control Systems Magazine 28 (2) (2008) 65–83.
[4] G. Schitter, P.J. Thurner, P.K. Hansma, Design and input-shaping control of a novel scanner for high-speed atomic force microscopy, Mechatronics 18 (5–6) (2008) 282–288.
[5] T. Ando, T. Uchihashi, T. Fukuma, High-speed atomic force microscopy for nano-visualization of dynamic biomolecular processes, Progress in Surface Science 83 (7–9) (2008) 337–437.
[6] S. Devasia, E. Eleftheriou, S.O.R. Moheimani, A survey of control issues in nanopositioning, IEEE Transactions on Control Systems Technology 15 (5) (2007) 802–823.
[7] H. Jung, D.G. Gweon, Creep characteristics of piezoelectric actuators, Review of Scientific Instruments 71 (4) (2000) 1896–1900.
[8] P. Ge, M. Jouaneh, Tracking control of a piezoceramic actuator, IEEE Transactions on Control Systems Technology 4 (3) (1996) 209–216.
[9] G.M. Clayton, S. Tien, K.K. Leang, Q. Zou, S. Devasia, A review of feedforward control approaches in nanopositioning for high-speed SPM, Journal of Dynamic Systems, Measurement, and Control 131 (6) (2009), 061101(1–19).
[10] K.K. Leang, S. Devasia, Feedback-linearized inverse feedforward for creep, hysteresis, and vibration compensation in AFM piezoactuators, IEEE Transactions on Control Systems Technology 15 (5) (2007) 927–935.
[11] D. Croft, G. Shed, S. Devasia, Creep, hysteresis, and vibration compensation for piezoactuators: atomic force microscopy application, ASME Journal of Dynamic Systems, Measurement, and Control 123 (1) (2001) 35–43.
[12] M. Rakotondrabe, C. Clevy, P. Lutz, Complete open loop control of hysteretic, creeped, and oscillating piezoelectric cantilevers, IEEE Transactions on Automation Science and Engineering 7 (3) (2010) 440–450.
[13] H. Jung, J.Y. Shim, D. Gweon, Tracking control of piezoelectric actuators, Nanotechnology 12 (1) (2001) 14–20.
[14] C.H. Ru, L.N. Sun, Improving positioning accuracy of piezoelectric actuators by feedforward hysteresis compensation based on a new mathematical model, Review of Scientific Instruments 76 (9) (2005) 095111.
[15] G.Y. Gu, L.M. Zhu, C.Y. Su, H. Ding, Motion control of piezoelectric positioning stages: modeling, controller design and experimental evaluation, IEEE/ASME Transactions on Mechatronics (2012), http://dx.doi.org/10.1109/TMECH.2012.2203315
[16] H.C. Liaw, B. Shirinzadeh, Robust adaptive constrained motion tracking control of piezo-actuated flexure-based mechanisms for micro/nano manipulation, IEEE Transactions on Industrial Electronics 58 (4) (2011) 1406–1415.
[17] A.J. Fleming, K.K. Leang, Charge drives for scanning probe microscope positioning stages, Ultramicroscopy 108 (12) (2008) 1551–1557.
[18] S. Salapaka, A. Sebastian, J.P. Cleveland, M.V. Salapaka, High bandwidth nano-positioner: a robust control approach, Review of Scientific Instruments 793 (9) (2002) 3232–3241.
[19] C. Visone, Hysteresis modelling and compensation for smart sensors and actuators, Journal of Physics: Conference Series 138 (1) (2008) 012028.
[20] R. Iyer, X. Tan, Control of hysteretic systems through inverse compensation, IEEE Control Systems Magazine 29 (1) (2009) 83–99.
[21] M. Rakotondrabe, Bouc-wen modeling and inverse multiplicative structure to compensate hysteresis nonlinearity in piezoelectric actuators, IEEE Transactions on Automation Science and Engineering 8 (2) (2011) 428–431.
[22] H. Hu, R.B. Mrad, A discrete-time compensation algorithm for hysteresis in piezoceramic actuators, Mechanical Systems and Signal Processing 18 (1) (2004) 169–185.
[23] D. Davino, C. Natale, S. Pirozzi, C. Visone, A fast compensation algorithm for real-time control of magnetostrictive actuators, Journal of Magnetism and Magnetic Materials 290–291 (2) (2005) 1351–1354.
[24] S.R. Viswamurthy, R. Ganguli, Effect of piezoelectric hysteresis on helicopter vibration control using trailing-edge flaps, Journal of Guidance, Control, and Dynamics 29 (5) (2006) 1201–1209.
[25] S. Viswamurthy, R. Ganguli, Modeling and compensation of piezoceramic actuator hysteresis for helicopter vibration control, Sensors and Actuators A: Physical 135 (2) (2007) 801–810.
[26] H. Janocha, K. Kuhnen, Real-time compensation of hysteresis and creep in piezoelectric actuators, Sensors and Actuators A: Physical 79 (2) (2000) 83–89.
[27] U.X. Tan, W.T. Latt, C.Y. Shee, C.N. Riviere, W.T. Ang, Feedforward controller of ill-conditioned hysteresis using singularity-free Prandtl–Ishlinskii model, IEEE/ASME Transactions on Mechatronics 14 (5) (2009) 598–605.
[28] M. Al Janaideh, S. Rakheja, C.Y. Su, An analytical generalized Prandtl–Ishlinskii model inversion for hysteresis compensation in micropositioning control, IEEE/ASME Transactions on Mechatronics 16 (4) (2011) 734–744.
[29] Y. Qin, Y. Tian, D. Zhang, B. Shirinzadeh, S. Fatikow, A novel direct inverse modeling approach for hysteresis compensation of piezoelectric actuator in feedforward applications, IEEE/ASME Transactions on Mechatronics 18 (3) (2013) 981–989.
[30] U. Tan, W.T. Latt, F. Widjaja, C.Y. Shee, C.N. Riviere, W.T. Ang, Tracking control of hysteretic piezoelectric actuator using adaptive rate-dependent controller, Sensors and Actuators A: Physical 150 (1) (2009) 116–123.
[31] B.A. Gozen, O.B. Ozdoganlar, A method for open-loop control of dynamic motions of piezo-stack actuators, Sensors and Actuators A: Physical 184 (2012) 160–172.
[32] G. Song, J.Q. Zhao, X.Q. Zhou, J.A. de Abreu-Garcia, Tracking control of a piezoceramic actuator with hysteresis compensation using inverse Preisach model, IEEE/ASME Transactions on Mechatronics 10 (2) (2005) 198–209.
[33] Q.S. Xu, P.K. Wong, Hysteresis modeling and compensation of a piezostage using least squares support vector machines, Mechatronics 21 (7) (2011) 1239–1251.
[34] Q.Q. Wang, C.Y. Su, Robust adaptive control of a class of nonlinear systems including actuator hysteresis with Prandtl–Ishlinskii presentations, Automatica 42 (5) (2006) 859–867.
[35] H.C. Liaw, B. Shirinzadeh, J. Smith, Enhanced sliding mode motion tracking control of piezoelectric actuators, Sensors and Actuators A: Physical 138 (1) (2007) 194–202.
[36] X.K. Chen, T. Hisayam, Adaptive sliding-mode position control for piezo-actuated stage, IEEE Transactions on Industrial Electronics 55 (11) (2008) 3927–3934.
[37] H. Liaw, B. Shirinzadeh, J. Smith, Robust motion tracking control of piezo-driven flexure-based four-bar mechanism for micro/nano manipulation, Mechatronics 18 (2) (2008) 111–120.
[38] C. Lee, S. Salapaka, Robust broadband nanopositioning: fundamental trade-offs, analysis, and design in a two-degree-of-freedom control framework, Nanotechnology 20 (3) (2009) 035501.
[39] N.N. Vorbringer-Dorozhovets, T. Hausotte, E. Manske, J.C. Shen, G. Jager, Novel control scheme for a high-speed metrological scanning probe microscope, Measurement Science and Technology 22 (9) (2011) 094012.
[40] Y.K. Yong, A.J. Fleming, S.O.R. Moheimani, A novel piezoelectric strain sensor for simultaneous damping and tracking control of a high-speed nanopositioner, IEEE/ASME Transactions on Mechatronics 18 (3) (2013) 1113–1121.
[41] G.Y. Gu, M.J. Yang, L.M. Zhu, Real-time inverse hysteresis compensation of piezoelectric actuators with a modified Prandtl–Ishlinskii model, Review of Scientific Instruments 83 (6) (2012) 065106.
[42] M. Al Janaideh, C.Y. Su, S. Rakheja, Development of the rate-dependent Prandtl–Ishlinskii model for smart actuators, Smart Materials and Structures 17 (3) (2008) 035026.
[43] X.L. Zhang, Y.H. Tan, A hybrid model for rate-dependent hysteresis in piezoelectric actuators, Sensors and Actuators A: Physical 157 (1) (2009) 54–60.
[44] P.K. Wong, Q.S. Xu, C.M. Vong, H.C. Wong, Rate-dependent hysteresis modeling and control of a piezostage using online support vector machine and relevance vector machine, IEEE Transactions on Industrial Electronics 59 (4) (2012) 1988–2001.
[45] G.Y. Gu, L.M. Zhu, Modeling of rate-dependent hysteresis in piezoelectric actuators using a family of ellipses, Sensors and Actuators A: Physical 165 (2) (2011) 202–209.
[46] M. Rakotondrabe, Y. Haddab, P. Lutz, Quadrilateral modeling and robust control of a nonlinear piezoelectric cantilever, IEEE Transactions on Control Systems Technology 17 (3) (2009) 528–539.

[47] Q. Li, W. Chen, Y. Wang, S. Liu, J. Jia, Parameter identification for PEM fuel-cell mechanism model based on effective informed adaptive particle swarm optimization, IEEE Transactions on Industrial Electronics 58 (6) (2011) 2410–2419.

Biographies

Guo-Ying Gu received the B.E. degree (with honors) in electronic engineering from Shanghai Jiao Tong University, Shanghai, China, in 2006, and the Ph.D. degree in mechanical engineering from Shanghai Jiao Tong University in 2012. He is currently working as a postdoctoral research fellow with School of Mechanical and Power Engineering at Shanghai Jiao Tong University. He was a Visiting Researcher with Department of Mechanical and Industrial Engineering at Concordia University, Montreal, QC, Canada from October 2010 to March 2011 and from November 2011 to March 2012. His research interests include modeling and control of smart material based actuators with hysteresis, and motion control of nanopositioning stages for scanning probe microscopy applications.

Li-Min Zhu received the B.E. degree (with honors) and the Ph.D. degree in mechanical engineering from Southeast University in 1994 and 1999, respectively. From November 1999 to January 2002, he worked as a postdoctoral fellow in Huazhong University of Science and Technology. In March 2002, he was appointed associate professor in the Robotics Institute, Shanghai Jiao Tong University. Since August 2005, he has been a professor. His research interests include (1) machining and inspection of complex shaped parts and (2) control, sensing and instrumentation for micro/nano manufacturing.